Skeletal Injuries Due to Behind Armour Blunt Trauma to the Spine

N. Hahne[1], E. Butler[1], KA. Carr[1], C. Howes[1], A. Rohrer[2], M. Clark[3], **A. Iwaskiw[1]**

[1]*The Johns Hopkins University Applied Physics Laboratory (JHU/APL), 11100 Johns Hopkins Road, Laurel, MD 20723, alexander.iwaskiw@jhuapl.edu*
[2] *Armed Forces Medical Examiner System, Defense Health Agency, Dover Air Force Base, DE*
[3] *U.S. Special Operations Command, 10 General Greene Avenue, Natick, MA 01760*

Abstract. Non-penetrating ballistic events inducing backface deformation in personal ballistic armour can cause blunt trauma to the human body. These deformation and injury patterns, known as behind armour blunt trauma (BABT), remain poorly understood. It is hypothesised that BABT directly over the spine could result in serious injury. In this study, live ammunition was used to strike ultra-high molecular weight polyethylene armour plates inducing BABT loading on instrumented postmortem human surrogates (PMHS). Nine tests were conducted using male PMHS specimens, with one ballistic plate per test. Impacts were delivered at near muzzle velocity. The 5th thoracic vertebral body was selected as the impact site, as it aligns with typical plate positioning under standard wear conditions. X-ray and computed tomography imaging were acquired before and after testing. Injury assessments were conducted through anatomical dissections by a board-certified forensic pathologist. Observed injuries ranged from superficial skin abrasions and lacerations to posterior element fractures, rib fractures, spinal cord impingement, and anterior vertebral body fractures. The PMHS model is limited in its ability to capture the functional outcome of these injuries, therefore it is of interest to compare these results with other biomechanical models that include living responses to these injuries. These findings highlight a potential risk of spinal injury from BABT and underscores the need to consider spinal trauma in future medical capability planning and ballistic armour design.

1. INTRODUCTION

The integration of advanced materials in contemporary personal armour design has significantly improved protection against ballistic penetration [1]. These designs strive to balance protection with weight reduction. While hard armour plates effectively stop ballistic projectiles, they can undergo significant backface deformation when stopping these threats. This rapid, high energy loading transfers energy through the plate to the body of the wearer potentially leading to behind armour blunt trauma (BABT), and resulting injuries can range from minor contusions to severe organ damage [2], [3]. In the interest of protecting military personnel, ongoing research aims to understand injury mechanisms, assess risks to the wearer, and evaluate the impact on operational readiness.

Relevant thresholds for maximum backface deformation (BFD) of ballistic armour plates is associated with 44 mm of deformation left in clay backing material, termed backface signature (BFS). This threshold was based on models that may not reflect the mechanisms of BABT on the human body accurately [4]. These standards were developed using in vivo animal surrogates and clay backed deformation studies to extrapolate human injury risk, however no direct relationship to human injury was established in these studies [1]. It is well documented that such animal models may not be representative of human injury risks for hard armour and clay does not accurately represent kinetic interactions between the armour and the body during impact, thus the risks of non-penetrating impacts to the wearer remain unclear [3], [5].

Typically, the same armour plate design is used to protect both the rear and front thoracic body regions. While this simplifies manufacturing considerations, this assumes that injury risk is equivalent for both locations. This assumption raises the question of whether the BFD standard for anterior impacts should be the same for posterior impacts. Understanding differences in vulnerability between the anterior and posterior thorax to blunt force loading is crucial for optimizing armour design [3], [5]. BABT to the anterior thorax has been modeled, and injury risk assessments indicate that such impacts can cause severe harm to the wearer [5], [6]. The potential impact of BABT over the spine is of particular concern given the risks to the spinal column and spinal cord. Computational modelling studies suggest that tissues beneath the armour experience pressure waves and shear deformation during BABT events, while animal studies indicate a risk of incapacitating injuries from such impacts [7], [8].

Epidemiological research on spinal injuries in both civilian and military populations has led to the development of several classification systems that help inform clinical implications and guide potential interventions [9], [10]. However, injuries associated with BABT involve unique mechanisms that remain

https://doi.org/10.52202/081621-0004

poorly understood in clinical practice and generally fall outside existing classification paradigms. This study introduces an experimental protocol utilizing instrumented post mortem human surrogates (PMHS), live ammunition, light weight hard ultra-high molecular weight polyethylene (UHMWPE) armour plates to induce BABT impacts to the thoracic spine. While numerous studies have examined the complex injury mechanisms of BABT in the thoracic region, this is the largest study to specifically investigate and characterise its effects on the thoracic spine in PMHS.

2. METHODS

2.1 Projectile and armour

All tests conducted in this study utilised the same projectile and armour pairing. Each plate was shot near muzzle velocity with a ballistic round relevant to current operational threats. The armour system investigated was designed to be standalone, therefore no backing material was used between the armour and test subject during impact. The armour was an UHMWPE composite multi-curved plate with a Small Arms Protective Insert (SAPI) shape. It was purposely developed to allow for large clay BFS under specific ballistic test conditions. Each plate was shot with the 7.62 x 51 mm M80 ball projectile to induce large backface deformation. The ballistic conditions selected for these tests were intended to induce associated BFS magnitudes around 60 mm. Each plate was tested once and shot 100 mm below the top edge along the mid-sagittal plane in line with the spinous process of the fifth thoracic vertebrae. Air gaps between the backside of the armour and the human anatomy at the point of impact ranged from 3.2-15.75 mm, and flesh thickness ranged from 12.4-39.8 mm. It is hypothesised that these local factors can affect loading to the skeleton.

2.2 PMHS demographics

Nine male, fresh frozen, full-body PMHS specimen were utilised for this study. All PMHS were acquired under institutional review board exemption approval through Johns Hopkins Medical Institution. PMHS were acquired with bilateral disarticulations at the distal femur. Specimens were selected using a specified range of metrics for age, stature, weight, body mass index (BMI) and lumbar bone mineral density (BMD) based on Dual Energy X-ray Absorptiometry (DEXA) imaging, Table 1. Specimen documented with prior trauma or severe thoracic disease were restricted from this study. Upon acquisition, specimens were imaged using computed tomography (CT) with slice thickness of 0.625 mm at the Johns Hopkins University Applied Physics Laboratory (JHU/APL) to ensure specimen had no prior trauma, medical interventions or thoracic conditions that could interfere with biomechanical testing or influence injury interpretation. To ensure that no specimens exhibited hyperkyphosis, the junctions between T1-T2 and T12-L1 were identified to measure the angle between these reference points using imaging software (3D Slicer 5.6.2 release). Specimens exceeding a kyphotic curvature of >40 degrees were classified as hyperkyphotic and excluded from the study. Specimen were stored at −20°C until thawed at 4°C six days prior to testing for instrumentation and test preparation.

Table 1. Specimen demographics

APL Identifier	Age	Cause of Death	Stature (cm)	Weight (kg)	BMI (kg/m^3)	DEXA (T-score)	Kyphosis Angle (degrees)
SPINE 01	56	Metoprolol/Amlodipine intoxication	188	108	30.7	2.4	34.8
SPINE 02	44	Brain tumour	191	100	27.5	0.5	38.8
SPINE 03	54	Hepatorenal syndrome	178	91	28.7	0.8	31.6
SPINE 04	63	Subdural hematoma	191	75	20.8	1.1	22.5
SPINE 05	49	Myocardial infarction	185	117	34.2	-1.2	32.0
SPINE 06	42	Cardiogenic shock, respiratory failure	165	65	23.8	-0.2	33.0
SPINE 07	42	Asphyxia	180	94	28.9	0.1	36.7
SPINE 08	45	Hepatic encephalopathy	178	106	33.4	-0.2	25.4
SPINE 09	33	Methamphetamine intoxication	175	94	30.6	2.4	33.1

2.3 PMHS instrumentation

While the focus of this study was on injury characterization rather than biomechanical analysis, each specimen was instrumented with biomechanical sensors to understand the mechanical and dynamic conditions during the ballistic event for use in future analyses. The techniques employed to affix sensors

were minimally invasive to avoid affecting injury outcomes resulting from BFD. Sensors were placed near anatomical regions proximal to the impact area and in organs of clinical interest shown in Table 2. The instrumentation employed included sternal motion, skeletal strain, skeletal acoustic emissions, organ pressure and surface contact.

Table 2. Specimen instrumentation

Sensor Description	Location	Type	Sensor	#
Rib strain	Posteriolateral ribs 4-9	Single axis strain gauge	Kyowa KFWB-2-350	12
Rib acoustic emission	Posteriolateral ribs 4-9	Acoustic emission sensor	Mistras Nano30	12
Lung pressure	Left and right bronchi	Pressure transducer	Kulite XCL-100- 100A	4
Vascular pressure	Aortic arch	Pressure transducer	Kulite XCL-100- 100A	1
Vascular pressure	Descending aorta (T11 vertebra)	Pressure transducer	Kulite XCL-100- 100A	1
Sternum acceleration	Superior manubrium and xiphoid	Single-axis accelerometer	Endevco 727	1
Surface force	On skin under armour	Contact sensor	TekScan flexiforce 301	5

Fluid was introduced into the cardiovascular system to simulate intravascular pressure. Foley catheters were guided through the carotid arteries, one catheter terminated at the aortic valve and a second terminated at the aortic junction. A third catheter was placed in the descending aorta at the level of the 11th thoracic vertebra superior to renal artery branches via femoral artery. Deployed foley catheter balloons allowed fluid to remain in the isolated vascular regions and contrast fluid was introduced to ensure proper sensor placement verified by CT. A tracheotomy was performed through which lung pressure sensors were introduced into the left and right primary bronchi and a tracheostomy tube was placed enabling lung insufflation with approximately 7 kPa of positive pressure during the test. CT was used to verify lungs were fully expanded and contacting the interior surface of the anterior plural wall. Post-instrumentation CT imaging was performed to document final sensor locations and lung insufflation.

2.4 PMHS experimental setup

After instrumentation, the PMHS were transported to a National Institute of Justice certified commercial ballistic test lab. The specimens were placed on a custom mounting rig allowing for the horizontally placed specimen to be rotated up right simulating a standing position. The specimens were strapped to the rig using nylon straps to support the head, arms and legs. The PMHS were supported by a straddle seat under the pubis, and foam material was used against the head and abdomen to offset the anterior thorax from the rig. The impact location was positioned along the mid-sagittal plane, over the spinous process of the fifth thoracic vertebra. Each specimen was placed upright and symmetrically on the rig and the rig was adjusted such that the impact location aligned with the ballistic target to simulate a rear shot over the targeted location on the spinal column (Figure 1).

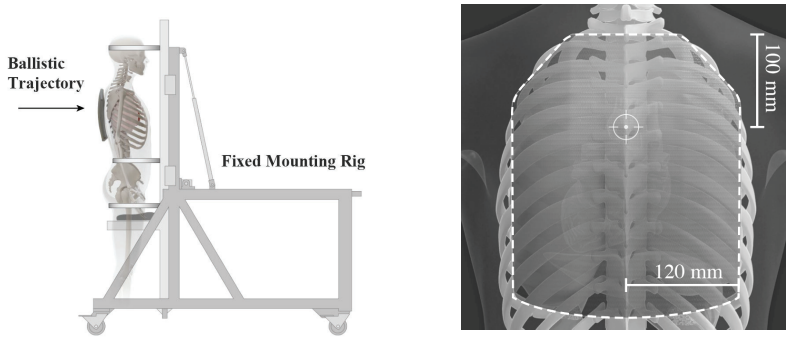

Figure 1. (Left) PMHS experimental setup. (Right) Schematic of armour alignment on specimen

The armour plate was aligned with the shot location on the specimen using a custom armour carrier with cutouts for the impact location to ensure no carrier material interferes with the BABT loading. The armour was donned to provide a “normal fit”, where the armour carrier was secured snugly to the specimen. Due to anatomical variability in the curvature of the upper rear torso, an airgap was present between the external surface of the skin and the backface of the plate. This backface standoff of the plate from the external surface of the skin at the anticipated point of impact was measured using a FARO arm (FARO Technologies, Lake Mary, Florida) by comparing the impact location on the PMHS before donning the armour to the impact location on the impact face of the armour after donning and

https://doi.org/10.52202/081621-0004

subtracting the armour thickness. The armour standoff was measured and ranged from 3-16 mm and obliquity spanned from -3° below to 16° relative to the horizontal plane. Pretest x-rays and photos were taken of the perfused and insufflated PMHS directly before the ballistic impact to ensure proper anatomical targeting and to measure sensor locations in situ (Figure 2).

BABT loading was subsequently induced by a single live-fire ballistic projectile. Velocity measurements were obtained using two sets of infrared screens (Oehler Research model No. 57) with universal counter chronographs (Hewlett-Packard model No. 53131A). Velocity was measured 4.6 m from the armour plate, and then velocity loss equations were applied specific to the projectile to calculate striking velocity.

While biomechanical characterization was not the focus of this study, high-rate data was acquired for use in future analysis. These metrics included acoustic emissions and strain from rib cage, vascular pressure and surface loading behind armour backface. Additionally, two high-speed camera systems (ACS-1-M60, NAC Image Technology) recorded the ballistic event from both a lateral and oblique view of the specimen at a rate of 100k and 50k frames per second respectively. All systems were simultaneously triggered with the signal disruption of a frangible break screen by the incoming round. All instrumentation signals, except acoustic emission data, were subject to a 300-kHz anti-alias filter.

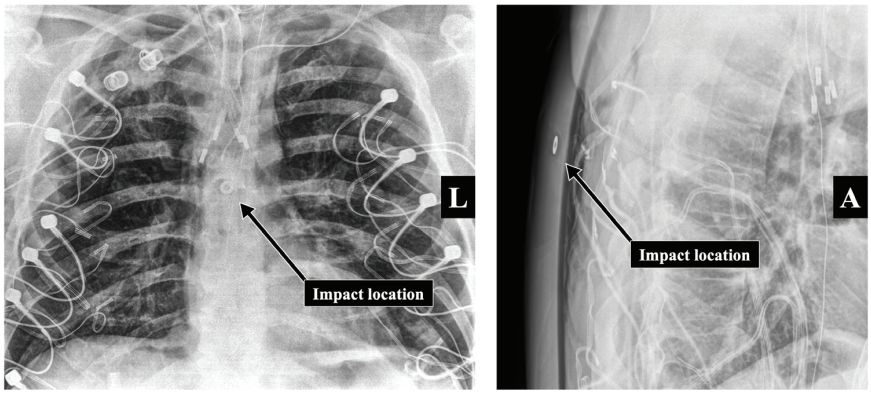

Figure 2. Characteristic specimen x-ray views of the thorax anteroposterior (left) and laterally (right) prior to impact (SPINE 03)

2.5 Post-test evaluation and forensic analysis

Immediately after each BABT loading event, post-test x-rays and photographs were taken without disruption of armour (Figure 3). Specimens were returned to a prone orientation and transported back to JHU/APL for post-test clinical CT imaging. Each specimen was scanned while in prone position with insufflated lungs with impacted armour in place and then scanned again with armour removed. The clinical CT imaging was reviewed by a board-certified forensic pathologist who subsequently led anatomical dissection of the PMHS. Dissection was conducted to document injury characteristics and evaluate injury severity. During this procedure, tissue layers were progressively reflected and organs removed sequentially for further analysis. Lungs were excised, inflated and inspected along with the chest wall for evidence of injury.

To visualise damage to the structural elements of the vertebral column, micro-computed tomography (μCT) was utilised (Nikon M2 Large Format). After the forensic analysis was completed, the spinal column from the second to the ninth thoracic vertebrae was disarticulated *en bloc* and μCT scanned at JHU/APL where each slice thickness was 75 μm providing six-fold increase in resolution compared the clinical CT modality. Finally, the vertebral bodies (anterior spinal column) were removed from the spinal column to visually examine the spinal cord and dural sheath (Cases SPINE 01-04).[1] Dissection observations were integrated into injury severity analysis using the Abbreviated Injury Scale (AIS). The AIS is a 7-digit, injury coding system that incorporates injury location, affected tissue and injury severity to calculate the New Injury Severity Score (NISS) [11]. The NISS is used to assess injury severity in the case where injury mechanisms induce polytrauma, and represents the sum of the square of the three most severe injuries occurring in a patient to be classified as mild (1-15), moderate (16-25),

[1] Removing the vertebral bodies was not routinely performed. This was a measured decision due to logistical considerations of obtaining initial micro CT imaging, the lack of significant spinal column intrusion by displaced bone, and understanding inherent limitations of identifying spinal cord injury in a PMHS.

https://doi.org/10.52202/081621-0004

severe (26-50) or critical (51-75) [12]. To quantify the most consequential injury, maximum abbreviated injury scale (MAIS) was used to compare cases.

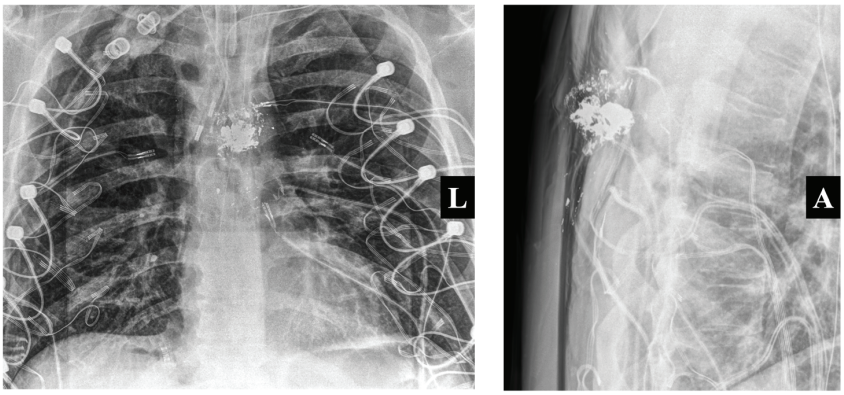

Figure 3. Characteristic specimen (SPINE 03) planar x-ray views of the thorax anteroposterior (left) and laterally (right) post impact visualizing the embedded projectile.

3. RESULTS

3.1 PMHS injuries

Injuries were observed in post-test medical imaging and during anatomical dissection. Representative images in Figure 4 and Figure 5 summarise extent of severe injury cases at T5. X-ray and clinical CT imaging demonstrate the residual armour deformation and resultant anatomical defects. μCT aided in visualizing vertebral fracture patterns for characterization. Associated injuries ranged from skin damage (AIS ≤ 1), pleural laceration (AIS 2), to multiple skeletal fractures (AIS ≤ 3). These injury outcomes can be found with corresponding injury codes in Appendix 1.

3.2 PMHS injury characteristics

The injuries observed at this impact location generally involved skin lacerations, ligament lacerations and skeletal fractures. All cases resulted in full thickness lacerations of the skin, exposing underlying tissue. These wounds ranged from approximately 6 -10 cm in width and 2 cm in depth. According to the NISS metric, these injuries are classified as 1, representing a minor injury severity. The second class of injury involved specific lacerations to the supraspinous ligament(s) and were broadly associated with

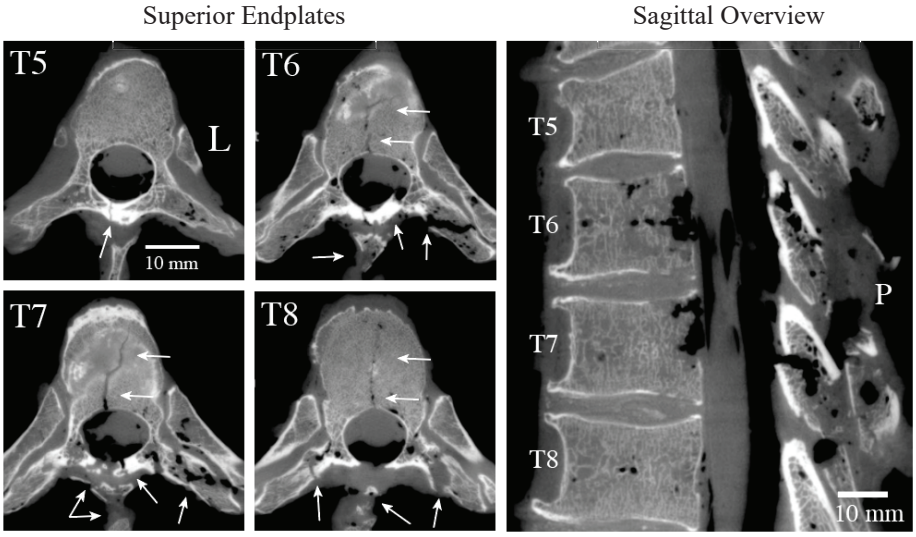

Figure 4. Resultant vertebral fractures from SPINE 04 post test

https://doi.org/10.52202/081621-0004

vertebral fractures. According to the NISS metric, these ligament injuries are classified as 1, also representing a minor injury severity.

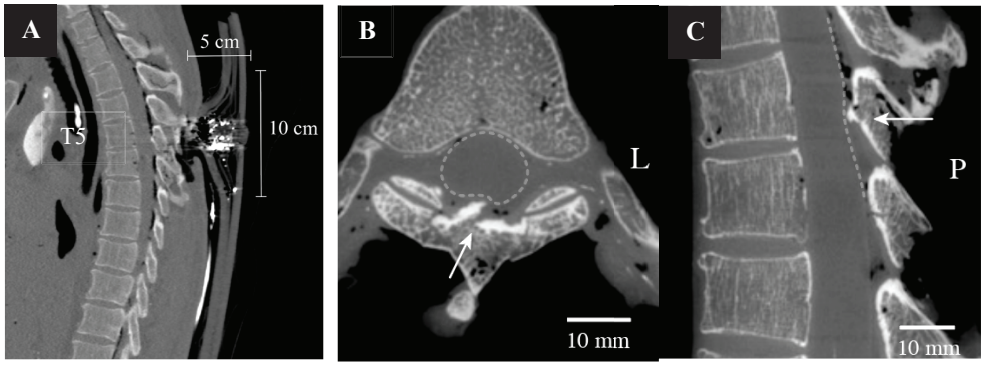

Figure 5. (A) Clinical CT scan showing lateral view of armour BFD spine intrusion. **(B)** and **(C)** Axial and lateral view (SPINE 06) of displaced fragments of vertebral fracture subsequent invasion into the vertebral foramen deforming the spinal cord (dotted line).

The third type of injury that was observed at this impact location were skeletal fractures involving the rib cage and vertebral segments. Rib cage fractures were identified in cases SPINE 02-04, 06-08 ranging from rib 5 to rib 8 and involved 2-3 ribs per case. Fractures generally occurred posteriorly with the exception of case SPINE 03 where anterior rib fractures were observed. These fractures included simple-nondisplaced, displaced and comminuted fracture patterns with simple-nondisplaced fractures occurring most frequently. AIS scoring for rib injury scales the severity according to the number of ribs involved. Injury involving 2 ribs is scored as 2 (moderate) and injuries involving 3 or more ribs are scored as 3 (serious).

The observed vertebral fractures involved the third through eighth thoracic vertebrae (T3-T8). In cases SPINE 01-04, 06-09, multiple vertebrae were fractured. These fracture patterns could be further characterised by the number of structural elements fractured and their location: (1) single fracture to a posterior vertebral element, (2) multiple fractures to posterior vertebral elements, (3) multiple fractures to posterior vertebral elements and vertebral body fracture (Figure 6). In order of prevalence, these included fractures of the spinous process, lamina, transverse process, vertebral body, superior articular facet, inferior articular facet and pedicle (Figure 7). Of the cases involving fractures, the most commonly fractured vertebrae were T6 and T7, with T6 sustaining the most fractures per case. T5, T6 and T7 were observed to have the largest variety of fracture types. The most common fractures involved the posterior elements of the vertebrae, namely the spinous process and lamina. A complete list of vertebral fractures can be found in Appendix 2.

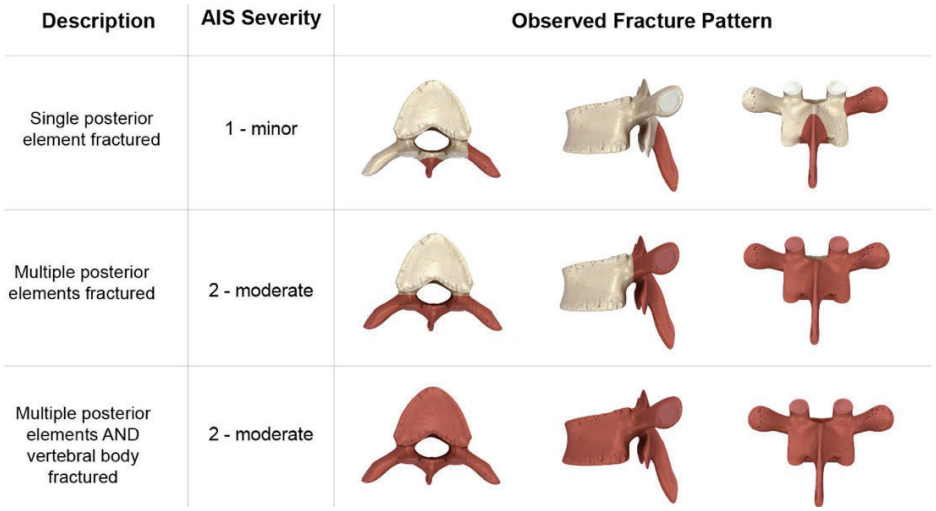

Figure 6. Illustration depicting the fracture patterns observed across all cases. Red areas indicate fractured regions.

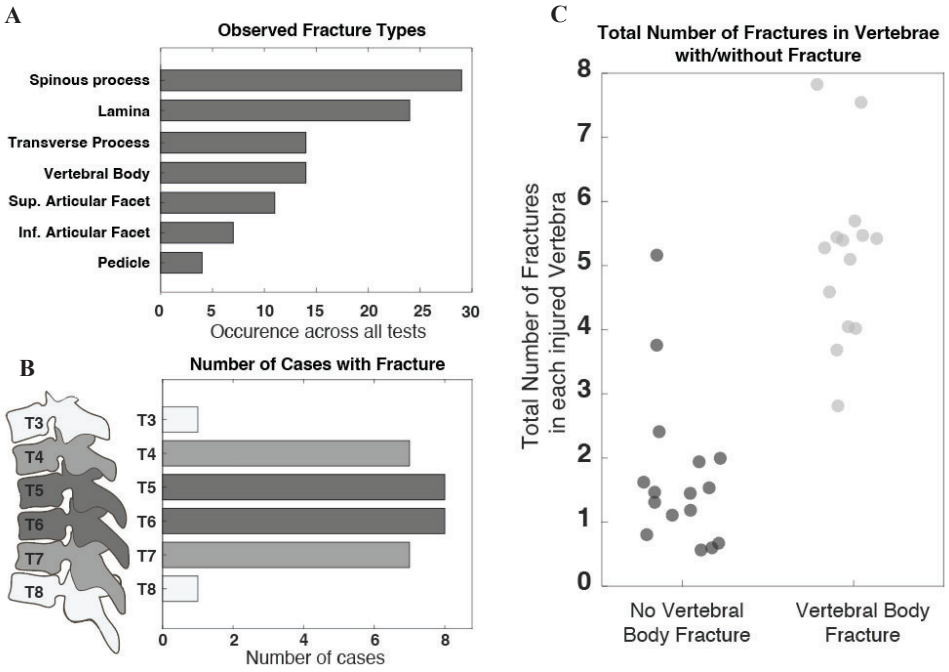

Figure 7. (A) Tabulation of all fracture types observed across all tests. **(B)** Distribution of fractures observed in injured vertebrae across all tests. **(C)** Fractures occurring in vertebrae with/without vertebral body fracture.

4. DISCUSSION

This ongoing study aims to characterise the breadth and severity of injuries resulting from BABT over the spine to inform clinical considerations and armour design policy. The clay BFS values in this study exceeds the 44 mm standard [1], the observed injuries represent a high-severity threshold for posterior BABT and approaches the ballistic penetration limit for this plate. We expect that providing data at these higher deformations provides critical insight into these injury mechanisms.

Fractures of the thoracic vertebrae are uncommon, accounting for only a small proportion of traumatic spinal injuries in both the general and military populations [10], [13]. The rib cage provides greater stability and rigidity to the thoracic vertebrae compared to other segments of the spinal column and are thus far more resistant to injury than the cervical and lumbar regions, regardless of impact mechanism [14]. For military personnel, spinal fractures are typically caused by falls or motor vehicle impacts. However, recent efforts have sought to better characterise combat-related spinal injury mechanisms [10], [15] . Isolated fractures of the posterior spinal elements are not typically associated with blunt trauma, whereas vertebral body fractures are commonly linked to compressive axial loading [12]. As an emerging threat with characteristically high velocity mechanics, the injuries observed in this study were unique and generally unobserved by the medical community. Notably, the third fracture pattern observed in this study involving destruction of vertebral posterior elements and vertebral body fracture was not represented in available datasets nor classification systems such as the widely adopted AO Spine Thoracolumbar spine injury system [16]. SPINE 03-04, 06-09 involved fractures of the vertebral body. This fracture pattern was associated with proximity to the impact location and correlated to a higher number of fractures per injured vertebrae (Figure 7). Since the anterior face of the vertebral bodies remained intact and no focal deformation was observed, it is possible that the posterior face of the vertebral body failed under tensile forces, appearing to be pulled apart.

To assess the severity of injury to the spinal column, this study utilised the AIS coding system. According to AIS conventions, each injured vertebral segment is assigned a specific code describing the fracture type and severity. Coding rules stipulate that the three most severe scores are used to tabulate a NISS score indicating overall injury severity. For multiple fractured vertebrae, the maximum severity score is 2 (moderate). Higher severity codes, up to 3 (serious), are available for vertebral injuries, but they specifically describe compression fractures resulting from axial loading. These classifications are inappropriate for this study, as BABT injuries involve posterior loading rather than axial compression.

https://doi.org/10.52202/081621-0004

Additionally, the NISS only accounts for the three most severe injuries and does not scale injury severity beyond three affected vertebral segments. Under this metric, the severity outcome for an individual remains the same if injury involves 3 or more than 3 vertebral segments. AIS scoring also differentiates between closed and open fractures, where open fractures involve penetrating injury mechanisms and are generally assigned a higher severity score. This creates a paradox in injury classification, as this study observed open fractures of the spine, yet BABT injuries do not result from penetrating trauma. This discrepancy complicates the development of an appropriate injury risk assessment framework.

4.1 Study limitations

The development of spinal cord injury due to BABT can be divided into primary and secondary phase. Primary injury is caused by BFD acting on the spinal column and the secondary injury is the resulting haemorrhage, ischemia and inflammation [17]. Critically, this PMHS experimental model is unable to resolve these secondary elements of spinal cord injury. Research has shown that impact velocity is a key factor in determining spinal cord injury severity [18]. Blunt trauma-induced spinal cord injuries can occur through direct deformation or contact with vertebral elements [19]. Animal studies suggest BABT in the thoracic spine can generate sufficient deformation inducing injurious pressures in the central nervous system and lung [8]. Although this study did not observe direct disruption of spinal dura, several cases (SPINE 03, 04, 06, 07) involved substantial vertebral fracture, leading to comminuted bone fragments invading the spinal canal and impinging the spinal cord (Figure 5). A critical component of future analysis of spine BABT injury risks will need to involve identifying mechanical pressure or shear loading in the spinal cord. This will enable development of a dose response model to compare to current models based on animal and computational studies.

This study attempted to utilise currently available injury scoring systems to characterise the severity of injuries observed in these experiments. But these systems have several fundamental shortcomings. AIS coding requires spinal cord injuries to be classified by neurological impairment and functional loss, which is not available in the PMHS model. These injury characteristics represent an emerging phenomenon associated with backface deformation in hard armour capable of stopping ballistic rounds. Characterizing these injuries and their clinical implications will be crucial for future injury risk analysis. However, the high-energy impact mechanisms involved in these cases complicate such analyses, as these injuries remain undefined within the medical community, leaving little clinical precedent for their evaluation. Current AIS-based injury severity assessments are insufficient, as they fail to capture the full spectrum of injury presentations and lack critical consideration of neurological injury risk.

5. CONCLUSIONS

This study introduced an experimental methodology and initial injury findings from nine live-fire, non-penetrating ballistic impacts on instrumented PMHS. Observations from each case revealed injuries ranging from minor skin lacerations to multiple fractures of adjacent vertebrae. The injured vertebrae exhibited distinct fracture patterns based on the affected elements: single posterior element fractures, multiple posterior element fractures, and multiple fractures involving the vertebral body. The extent of substantial vertebral fracture correlated with impact proximity, while vertebral body involvement was associated with a higher number of fractures per vertebra. These findings contribute to an ongoing effort to better understand the factors influencing BABT injury risk and to inform future armour design standards. Additionally, because of the extent of fractures in the vertebral bodies, it is recommended that future studies utilise a human surrogate with a living tissue response (i.e. animal). By quantifying the injury risks associated with BABT to the posterior thorax, this study highlights the need for armour designs tailored specifically for rear protection. These observations suggest that rear-impact BABT presents unique injury patterns that warrant considerations for modifying armour design or performance standards. Currently fielded plates are designed to a standard based on clay deformation rather than actual injury observations. Here we present a data set that facilitates shifting from traditional armour design philosophies toward an evidence-based approach that accounts for regional injury vulnerability. Integrating these findings into armour standards will enhance survivability and operational effectiveness for personnel in combat environments.

Acknowledgments

The authors would like to express their appreciation to the U.S. Special Operations Command for funding this work under Contract No. is H92222-15-D-0004.

References

[1] E. Hanlon and et al, "Origin of the 44-mm Behind-Armor Blunt Trauma Standard," *Military Medicine,* vol. 177, no. 3, pp. 333-339, 2012.

[2] N. Pratt and et al, " Contemporary body armor: technical data, injuries, and limits," *European Journal of Trauma and Emergency Surgery,* vol. 38, no. 2, pp. 95-105, 2012.

[3] V. Kote and et al, "Investigating the Impact of Blunt Force Trauma: A Probabilistic Study of Behind Armor Blunt Trauma Risk," *Annals of Biomedical Engineering,* 2025.

[4] U. D. o. Justice, "Ballistic resistance of police body armor," *National Institute of Justice,* pp. 1-13, 1986.

[5] C. Bass and et al, "Injury Risk in behind armor blunt thoracic trauma," *International Journal of Occupational Safety and Ergonomics,* vol. 12, no. 4, pp. 429-442, 2006.

[6] A. Iwaskiw and et al, "Initial injury observations in postmortem human subjects: Non-penetrating ballistic impacts over the sternum with lightweight hard armour plates," in *Personal Armour Systems Symposium*, Copenhagen, 2021.

[7] A. Merkle and et al, " Assessing behind armor blunt trauma (BABT) under NIJ Standard-0101.04 conditions using human torso models," *Journal of Trauma-Infection and Critical Care,* vol. 64, no. 6, pp. 1555-1561, 2008.

[8] B. Zhang and et al, " Neurological, Functional, and Biomechanical Characteristics After High-Velocity Behind Armor Blunt Trauma of the Spine," *Journal of Trauma-Injury Infection and Critical Care,* vol. 71, no. 6, pp. 1680-1688, 2011.

[9] J. Blair and et al, " Military penetrating spine injuries compared with blunt," *Spine Journal,* vol. 12, no. SI, pp. 762-768, 2012.

[10] K. Holly and et al, "Spinal Injuries and Spine Care in the US Military Health System (2001-Present)," *Spine,* vol. 50, no. 2, pp. 207-215, 2025.

[11] AAAM, "Abbreviated Injury Scale (AIS)," *Association fo the Advancement of Automotive medicine,* pp. xx-xix, 2015.

[12] K. Aghkhani and et al, "The association between type of spine fracture and the mechanism of trauma: A useful tool for identifying mechanism of trauma on legal medicine field," *Journal of Forensic and Legal Medicine,* vol. 56, no. 56, pp. 80-82, 2018.

[13] J. Holmes and et al, "Epidemiology of thoracolumbar spine injury in blunt trauma," *Academic Emergency Medicine,* vol. 8, no. 9, pp. 866-872, 2001.

[14] U. Spiegl and et al, "Traumatic Fractures of the Thoracic Spine: Narrative Literature Review," *Zeitschrift fur Orthopadie und Enfallchirurgie,* vol. 159, no. 4, pp. 373-382, 2021.

[15] N. Szuflita and et al, "Spine Injuries Sustained by US Military Personnel in Combat Are Different From Non-Combat Spine Injuries," *Military Medicine,* vol. 181, no. 10, pp. 1314-1323, 2016.

[16] A. Vaccaro and et al, "The surgical algorithm for the AOSpine thoracolumbar spine injury classification system," *European Journal,* vol. 25, no. 4, pp. 1087-1094, 2016.

[17] N. Nishida and et al, "Tensile mechanical analysis of anisotropy and velocity dependence of the spinal cord white matter: a biomechanical study," *Neural Regeneration Research,* vol. 16, no. 12, pp. 2557-2562, 2021.

[18] S. Mattucci and et al, "Basic biomechanics of spinal cord injury - How injuries happen in people and how animal models have informed our understanding," *Clinical Biomechanics,* vol. 64, no. SI, pp. 58-68, 2019.

[19] C. Jones and E. Clarke, "Engineering approaches to understanding mechanisms of spinal column injury leading to spinal cord injury," *Clinical Biomechanics,* vol. 64, no. SI, pp. 69-81, 2019.

Appendix 1: AIS Injury Coding (fx = fracture, w/o = without)

Identifier	AIS Code	AIS Description	NISS	MAIS
SPINE 01	410202.1; 410602.1	Skin; abrasion; laceration	12	2
	640484.1	Spinous ligament injury, thoracic spine		
	650410.2	Vertebra, thoracic, dislocation no cord involvement, facet, unilateral		
	650417.2	Vertebra, thoracic, fx w/o neurologic deficit, multiple fx of same vertebra		

https://doi.org/10.52202/081621-0004

	650418.1	Vertebra, thoracic, fx w/o neurologic deficit, spinous process		
SPINE 02	410202.1; 410602.1	Skin; abrasion; laceration	12	2
	450202.2	Rib cage, fx w/o flail, any location unilateral or bilateral, two ribs		
	640484.1	Spinous ligament injury, thoracic spine		
	650417.2	Vertebra, thoracic, fx w/o neurologic deficit, multiple fx of same vertebra		
	650418.1	Vertebra, thoracic, fx w/o neurologic deficit, spinous process		
	650420.1	Vertebra, thoracic, fx w/o neurologic deficit, multiple fx of same vertebra		
SPINE 03	410202.1; 410602.1	Skin; abrasion; laceration	12	2
	450202.2	Rib cage, fx w/o flail, any location unilateral or bilateral, two ribs		
	640484.1	Spinous ligament injury, thoracic spine		
	650417.2	Vertebra, thoracic, fx w/o neurologic deficit, multiple fx of same vertebra		
	650418.1	Vertebra, thoracic, fx w/o neurologic deficit, spinous process		
SPINE 04	410202.1; 410602.1	Skin; abrasion; laceration	17	3
	441800.2	Pleura laceration		
	450203.3	Rib cage, fx w/o flail, any location unilateral or bilateral, >=3 ribs		
	650417.2	Vertebra, thoracic, fx w/o neurologic deficit, multiple fx of same vertebra		
	650418.1	Vertebra, thoracic, fx w/o neurologic deficit, multiple fx of same vertebra		
SPINE 05	410202.1; 410602.1	Skin; abrasion; laceration	2	1
SPINE 06	410202.1; 410602.1	Skin; abrasion; laceration	17	3
	450203.3	Rib cage, fx without flail, any location unilateral or bilateral, >=3 ribs		
	650417.2	Vertebra, thoracic, fx w/o neurologic deficit, multiple fx of same vertebra		
SPINE 07	410202.1; 410602.1	Skin; abrasion; laceration	17	3
	450203.3	Rib cage, fx w/o flail, any location unilateral or bilateral, >=3 ribs		
	640484.1	Spinous ligament injury; thorax, laceration, minor; superficial		
	650417.2	Vertebra, thoracic, fx w/o neurologic deficit, multiple fx of same vertebra		
	650418.1	Vertebra, thoracic, fx w/o neurologic deficit, spinous process		
SPINE 08	410202.1; 410602.1	Skin; abrasion; laceration	17	3
	450203.3	Rib cage, fx w/o flail, any location unilateral or bilateral, >=3 ribs		
	640484.1	Spinous ligament injury; thorax, laceration, minor; superficial		
	650417.2	Vertebra, thoracic, fx w/o neurologic deficit, multiple fx of same vertebra		
	650418.1	Vertebra, thoracic, fx w/o neurologic deficit, spinous process		
SPINE 09	410202.1; 410602.1	Skin; abrasion; laceration	9	2
	640484.1	Spinous ligament injury, thoracic spine		
	650417.2	Vertebra, thoracic, fx w/o neurologic deficit, multiple fx of same vertebra		
	650418.1	Vertebra, thoracic, fx w/o neurologic deficit, spinous process		

Appendix 2: Vertebral Fractures (Sup = Superior, Inf = Inferior)

Identifier	Vertebra	Description
SPINE 01	T4	Spinous process
	T5	Spinous process
	T6	Lamina (comminuted); Spinous process (comminuted)
	T7	Lamina (comminuted); Spinous process (comminuted)
SPINE 02	T4	Spinous process
	T5	Lamina; spinous process
	T6	R pedicle; R transverse process; Lamina; Spinous process
	T7	R transverse process
SPINE 03	T4	Spinous process
	T5	Laminal; spinous process
	T6	Vertebral body; R pedicle; R transverse process; Lamina; Spinous process (comminuted/avulsed)
	T7	Vertebral body; R pedicle; R/L transverse process; Lamina; Spinous process (comminuted/avulsed)
SPINE 04	T4	Spinous process tip
	T5	R lamina into spinous process; Spinous process (comminuted/displaced)
	T6	Vertebral body; L lamina; L/R transverse processes; Spinous process
	T7	Vertebral body; L/R Sup articular facet; L/R transverse process; Spinous process; L/R Inf articular facet
	T8	Vertebral body; L/R Sup articular facet; L/R transverse process; Spinous process; L/R Inf articular facet
SPINE 05	T5	Spinous process; L Sup articular facet fracture; Vertebral body; L/R lamina (comminuted)
	T6	Vertebral body; Spinous process (comminuted); R Inf articular facet; L/R lamina
	T7	R Sup articular facet; spinous process
SPINE 06	T4	Spinous process
	T5	Vertebral body; L/R lamina; Spinous process
	T6	Vertebral body; L/R lamina; Left transverse process; Spinous process
	T7	Vertebral body; L/R lamina; Left transverse process; Spinous process
SPINE 07	T3	Spinous process
	T4	Spinous process
	T5	R pedicle; R lamina; R transverse process; R Inf facet; Spinous process
	T6	L/R Sup articular facet; Vertebral body; Midline lamina; Spinous process
	T7	R Sup facet; L/R Sup articular facet; Lamina (comminuted); Vertebral body
SPINE 09	T4	Spinous process
	T5	Vertebral body; Midline lamina; Spinous process (comminuted)
	T6	Vertebral body; Midline lamina; L Inf facet; Spinous process (comminuted)